LYMPHATICS

Pathogenic variants in *MDFIC* cause recessive central conducting lymphatic anomaly with lymphedema

Alicia B. Byrne[1,2]†, Pascal Brouillard[3]†, Drew L. Sutton[1]†, Jan Kazenwadel[1]†, Saba Montazaribarforoushi[4]‡, Genevieve A. Secker[1]‡, Anna Oszmiana[1], Milena Babic[1,5], Kelly L. Betterman[1], Peter J. Brautigan[1,5], Melissa White[4,6,7], Sandra G. Piltz[4,6,7], Paul Q. Thomas[4,6,7], Christopher N. Hahn[1,4,5,8], Matthias Rath[9], Ute Felbor[9], G. Christoph Korenke[10], Christopher L. Smith[11,12], Kathleen H. Wood[13], Sarah E. Sheppard[14], Denise Adams[15], Ariana Kariminejad[16], Raphael Helaers[3], Laurence M. Boon[3,17], Nicole Revencu[17,18], Lynette Moore[19], Christopher Barnett[20], Eric Haan[4], Peer Arts[1], Miikka Vikkula[3,17,18,21]*§, Hamish S. Scott[1,4,5,8]*§, Natasha L. Harvey[1,4]*§

Central conducting lymphatic anomaly (CCLA), characterized by the dysfunction of core collecting lymphatic vessels including the thoracic duct and cisterna chyli, and presenting as chylothorax, pleural effusions, chylous ascites, and lymphedema, is a severe disorder often resulting in fetal or perinatal demise. Although pathogenic variants in RAS/mitogen activated protein kinase (MAPK) signaling pathway components have been documented in some patients with CCLA, the genetic etiology of the disorder remains uncharacterized in most cases. Here, we identified biallelic pathogenic variants in *MDFIC*, encoding the MyoD family inhibitor domain containing protein, in seven individuals with CCLA from six independent families. Clinical manifestations of affected fetuses and children included nonimmune hydrops fetalis (NIHF), pleural and pericardial effusions, and lymphedema. Generation of a mouse model of human *MDFIC* truncation variants revealed that homozygous mutant mice died perinatally exhibiting chylothorax. The lymphatic vasculature of homozygous *Mdfic* mutant mice was profoundly mispatterned and exhibited major defects in lymphatic vessel valve development. Mechanistically, we determined that MDFIC controls collective cell migration, an important early event during the formation of lymphatic vessel valves, by regulating integrin β_1 activation and the interaction between lymphatic endothelial cells and their surrounding extracellular matrix. Our work identifies *MDFIC* variants underlying human lymphatic disease and reveals a crucial, previously unrecognized role for MDFIC in the lymphatic vasculature. Ultimately, understanding the genetic and mechanistic basis of CCLA will facilitate the development and implementation of new therapeutic approaches to effectively treat this complex disease.

INTRODUCTION

Lymphatic vessels fulfill crucial roles in tissue fluid homeostasis, dietary lipid absorption, and the direction of immune cell traffic (*1*, *2*). Defects in construction of the lymphatic vasculature during embryonic development often result in devastating outcomes including fetal or perinatal death, largely due to the detrimental impact of excessive fluid accumulation on pulmonary and cardiac development and function (*3*). Central conducting lymphatic anomaly (CCLA), in which the development and function of large, truncal collecting lymphatic vessels is affected, is a severe lymphatic malformation for which few effective treatments are available (*3*–*5*). Recent work revealed a recurrent, gain-of-function pathogenic variant in *ARAF*, affecting activity of the RAS/mitogen activated protein kinase (MAPK) signaling pathway, underlying CCLA (*6*), and pathogenic variants in RAS/MAPK pathway genes including *PTPN11*, *KRAS*, *BRAF*, *SOS1*, *HRAS*, *ARAF*, *RAF1*, *CBL*, *RIT1*, and *RASA1* are established to cause developmental lymphatic vascular malformations manifesting in chylothorax (the accumulation of lipid-rich chyle in the thoracic cavity caused by lymphatic vessel dysfunction), pleural or pericardial effusions, lymphangiectasia, and lymphedema (*6*–*15*).

[1]Centre for Cancer Biology, University of South Australia and SA Pathology, 5001 Adelaide, Australia. [2]Clinical and Health Sciences, University of South Australia, 5001 Adelaide, Australia. [3]Human Molecular Genetics, de Duve Institute, University of Louvain, 1200 Brussels, Belgium. [4]Adelaide Medical School, University of Adelaide, 5005 Adelaide, Australia. [5]Department of Genetics and Molecular Pathology, SA Pathology, 5000 Adelaide, Australia. [6]Genome Editing Program, South Australian Health and Medical Research Institute, 5000 Adelaide, Australia. [7]South Australian Genome Editing Facility, University of Adelaide, 5005 Adelaide, Australia. [8]ACRF Cancer Genomics Facility, Centre for Cancer Biology, University of South Australia and SA Pathology, 5001 Adelaide, Australia. [9]Department of Human Genetics, University Medicine Greifswald and Interfaculty Institute of Genetics and Functional Genomics, University of Greifswald, 17489 Greifswald, Germany. [10]Department of Neuropediatrics, University Children's Hospital, Klinikum Oldenburg, 26133 Oldenburg, Germany. [11]Jill and Mark Fishman Center for Lymphatic Disorders, Children's Hospital of Philadelphia, Philadelphia, PA 19104, USA. [12]Division of Cardiology, Children's Hospital of Philadelphia and Department of Pediatrics Perelman School of Medicine at The University of Pennsylvania, Philadelphia, PA 19104, USA. [13]Division of Genomic Diagnostics, Children's Hospital of Philadelphia, Philadelphia, PA 19104, USA. [14]Division of Human Genetics, Children's Hospital of Philadelphia, Philadelphia, PA 19104, USA. [15]Vascular Anomalies Centre, Division of Haematology/Oncology, Cancer and Blood Disorders Centre, Boston Children's Hospital, Boston, PA 02115, USA. [16]Kariminejad-Najmabadi Pathology and Genetics Centre, Tehran, Iran. [17]Center for Vascular Anomalies, Division of Plastic Surgery, VASCERN VASCA European Reference Centre, Cliniques Universitaires Saint-Luc and University of Louvain, 1200 Brussels, Belgium. [18]Centre for Human Genetics, Cliniques Universitaires Saint-Luc and University of Louvain, 1200 Brussels, Belgium. [19]Department of Surgical Pathology, SA Pathology, 5000 Adelaide, Australia. [20]Paediatric and Reproductive Genetics Unit, South Australian Clinical Genetics Service, Women's and Children's Hospital, 5006 Adelaide, South Australia, Australia. [21]Walloon Excellence in Life Sciences and Biotechnology, University of Louvain, 1200 Brussels, Belgium.
*Corresponding author. Email: miikka.vikkula@uclouvain.be (M.V.); hamish.scott@sa.gov.au (H.S.S.); natasha.harvey@unisa.edu.au (N.L.H.)
†These authors contributed equally to this work.
‡These authors shared second authorship.
§These authors contributed equally to this work.

Identification of the activating mutations in *ARAF* and *KRAS* underlying CCLA and complicated lymphatic anomaly (CLA) enabled treatment for some patients with the MAPK kinase (MEK) inhibitor trametinib, resulting in marked improvement of their debilitating lymphatic symptoms (*6*, *14*). These findings underscore the importance of defining the genetic and mechanistic basis of human disease in paving the way toward novel therapeutic strategies. Although our understanding of the genetics underlying human lymphatic vascular disease is rapidly advancing, the genetic etiology of lymphatic vascular anomalies remains enigmatic in most cases (*7*, *15*, *16*).

Lymphatic vascular development commences in the embryo when expression of the master transcriptional regulator of lymphatic endothelial cell identity, *Prox1*, is initiated in a population of endothelial cells within the cardinal and intersomitic veins (*17*, *18*). PROX1-positive lymphatic endothelial progenitor cells elevate their expression of factors important for lymphatic vascular development, including vascular endothelial growth factor receptor 3 (VEGFR3), neuropilin 2 (NRP2), and podoplanin (PDPN), upon sprouting and exit from the veins (*18*, *19*) and migrate in a manner dependent on the VEGFR3 ligand, vascular endothelial growth factor C (VEGFC) (*20*), to form the initial truncal lymphatic vascular structures in the embryo. These initial lymphatic sacs and plexuses undergo marked expansion, remodeling, and juxtaposition, to generate an interconnected lymphatic vascular network (*21*). An important aspect of lymphatic vessel maturation is the development of lymphatic vessel valves, which act to ensure that lymph is returned efficiently in a unidirectional manner to the bloodstream (*22*). Valve development is dependent on key transcription factors including FOXC2 (*23*–*25*) and GATA2 (*26*, *27*), abundance of which is elevated in valve-forming territories in response to flow-initiated signals (*26*). The failure of lymphatic vessel valves to form or function in mice deficient in genes including *Foxc2* and *Gata2*, or harboring a pathogenic variant in *Kras*, results in lymphatic phenotypes including edema, chylous ascites, and chylothorax (*14*, *23*, *26*, *28*). Patients with primary lymphedema syndromes or lymphatic malformations caused by pathogenic variants in *FOXC2*, *GATA2*, or *KRAS* also exhibit lymphatic vessel valve defects and, in some cases, venous valve defects, underscoring the impact of valve defects on lymphatic function in human lymphatic disease (*14*, *23*, *29*, *30*).

MDFIC encodes the MyoD family inhibitor domain containing protein, a 246–amino acid protein (*31*) documented to regulate the activity of transcription factors including the glucocorticoid receptor (GR) (*32*), HAND1 (*33*), and T cell factor/lymphoid enhancer factor (TCF/LEF) family members (*34*, *35*). The C-terminal region of MDFIC harbors a domain extremely rich in cysteine residues, reported to mediate protein-protein interactions between MDFIC and transcription factor componentry (*31*–*35*). In this manner, MDFIC is proposed to tether transcription factors in the cytoplasm where MDFIC predominantly resides, thereby restricting their nuclear access and transcriptional activity. To date, the roles of MDFIC remain enigmatic, and *MDFIC* has not been implicated in cardiovascular development. Here, we report novel homozygous, and compound heterozygous, pathogenic variants in *MDFIC* in individuals with CCLA. Patients exhibited phenotypes including NIHF and stillbirth, or NIHF followed by postnatal lymphedema and pleural and pericardial effusions. Generation of a mouse model of the human frameshift *MDFIC* variant p.(Met131Asnfs*3), found in five of seven participants in our study, revealed that homozygous *Mdfic* pathogenic variants resulted in perinatal and postnatal death as a result of chylothorax caused by severe lymphatic vascular defects. Our data reveal that biallelic *MDFIC* pathogenic variants underlie CCLA and pave the way for the development of novel therapeutics to effectively treat this devastating disorder.

RESULTS

Identification of MDFIC pathogenic variants in patients with NIHF, postnatal lymphedema, and pleural and pericardial effusions

Genome sequencing or exome sequencing was performed to investigate the genetics underlying stillbirth, nonimmune hydrops fetalis (NIHF), and primary lymphedema in both diagnostic and research settings. In family LE-452 with two siblings exhibiting severe NIHF, filtering for rare, protein-altering variants revealed compound heterozygous variants in *MDFIC* in both affected children; a paternally inherited Chr7(hg19):g.114619728C>CA; NM_001166345.1:c.391dup; NP_001159817.1: p.Met131Asnfs*3 and a maternally inherited g.114655980 T>G; c.732 T>G; p.Phe244Leu (Fig. 1, A to C). The frameshift variant p.Met131Asnfs*3 leads to a premature termination codon and is reported in gnomAD (v2.1) 50 times in heterozygosity (popmax allele frequency 0.026%) with no homozygous occurrences (*36*). Similarly, the p.Phe244Leu missense variant has only been observed in gnomAD in heterozygosity (25 times, popmax allele frequency 0.13%). This variant is also predicted to be deleterious by in silico prediction tools including CADD (24.9), Polyphen2 (probably damaging), and SIFT (damaging), and altogether by 8 of 11 prediction tools in Varsome.

We subsequently identified homozygous truncating variants in *MDFIC* in probands from four consanguineous families and one nonconsanguineous family, all of whom displayed phenotypes consistent with CCLA (Table 1). Probands in families LE-410, LE-590, and CHOP-1 were homozygous for the p.Met131Asnfs*3 variant identified in family LE-452 (Fig. 1A). The parents of family LE-410 and CHOP-1 were heterozygous for this variant; however, those of family LE-590 were unavailable for testing. In family LE-230, the proband was homozygous for a p.Ser124* variant [Chr7(GRCh37): g.114619713TC>T; NM_001166345.1: c.371del], which results in a premature termination codon and is absent from gnomAD (Fig. 1, A to C). Both parents were heterozygous for the variant. In the final family (G764), the proband was homozygous for a p.Gly63* variant [Chr7(GRCh37):g.114582422G>T; NM_001166345.1:c.187G>T], for which both parents were heterozygous (Fig. 1, A to C). This variant results in a premature termination codon and is also absent from gnomAD.

Clinical presentation

The major clinical features of the seven patients (six families) are presented in Table 1. Each family is described in brief below. According to the International Society for the Study of Vascular Anomalie (ISSVA) 2018 classification, all cases had phenotypes consistent with a diagnosis of CCLA.

Family LE-452

The male proband (Fig. 1A; II.1) was the first child of nonconsanguineous Chinese parents. Hydrops fetalis was observed at the 19-week antenatal ultrasound. The male fetus was delivered at 26 weeks gestational age by caesarean section because of deteriorating fetal Dopplers. He

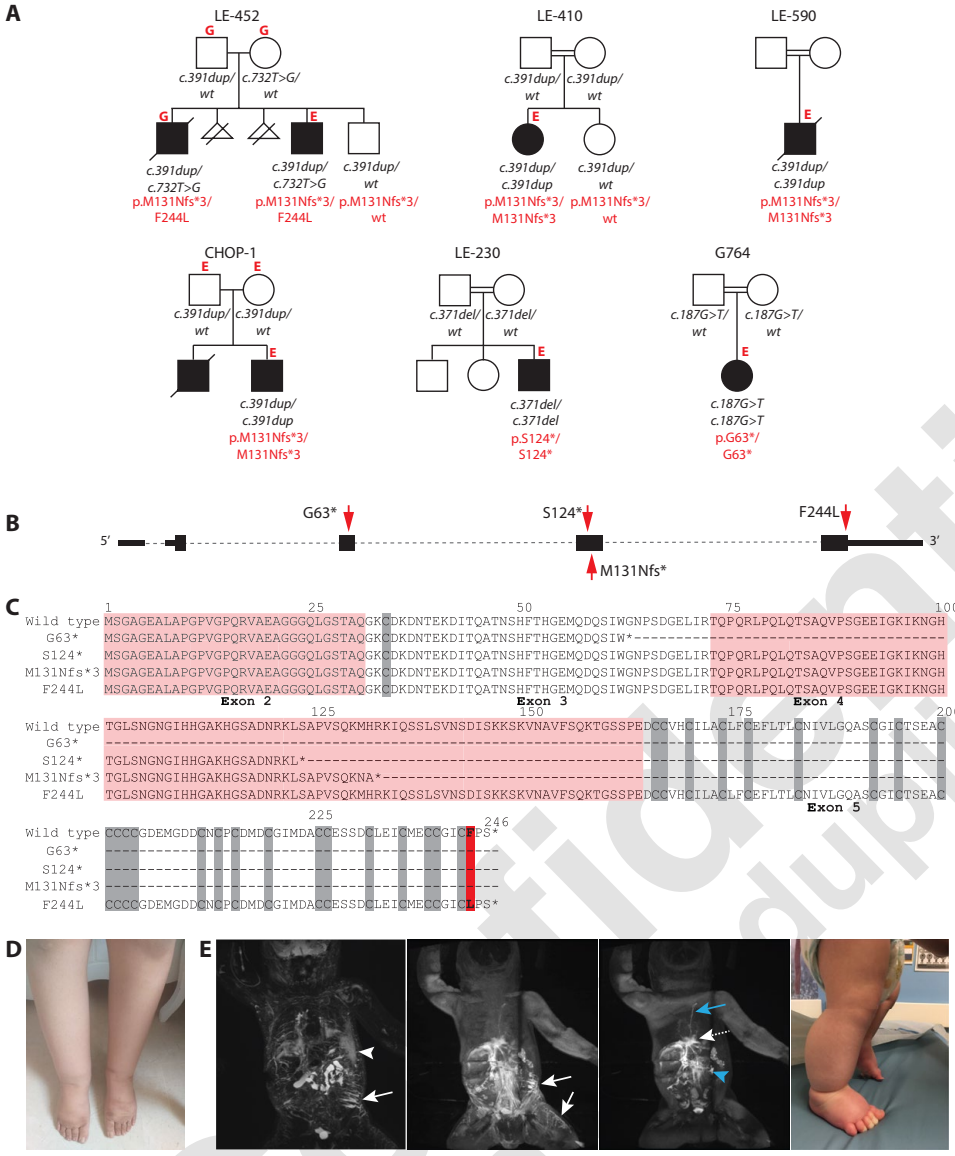

Fig. 1. Identification of *MDFIC* pathogenic variants in patients with fetal hydrops, postnatal lymphedema, and pleural and pericardial effusions. (**A**) Family pedigrees of children diagnosed with hydrops fetalis, pleural or pericardial effusions, and lymphedema. Pathogenic variants in the *MDFIC* gene sequence are indicated in black type, and corresponding MDFIC protein changes in red. Affected individuals are shown in black. Sequencing method is designated (E, exome; G, genome). (**B**) Schematic depicting exon/intron structure of *MDFIC* transcript. Exons are shown as black boxes, and patient variants are shown with red arrows. (**C**) Human MDFIC sequence alignment comparing wild-type (WT) and mutant proteins found in patients. Cysteine residues are highlighted in gray, and the F244L amino acid substitution in red. The region of MDFIC protein encoded by each exon is shaded alternately in pale red or white. (**D**) Photograph of lymphedema and papillomatosis in proband of LE-410. (**E**) Pleural effusions (white arrowhead), large cutaneous lymphatic channels (arrows), retrograde mesenteric lymphatic flow (blue arrowhead), dilated thoracic duct (blue arrow), and perfusion of the capsular lymphatics (dashed white arrow) visualized using T2-weighted magnetic resonance imaging, intranodal-dynamic contrast-enhanced magnetic resonance lymphangiography, and intrahepatic-dynamic contrast-enhanced magnetic resonance lymphangiography, respectively, together with lymphedema (photograph), in the proband of CHOP-1.

could not be resuscitated and died soon after birth. Autopsy documented severe NIHF, with subcutaneous edema, pericardial effusion, and bilateral pleural effusions and ascites, associated with severe pulmonary hypoplasia and an edematous placenta. Investigations at autopsy failed to find a cause for the hydrops. The two subsequent pregnancies for the couple were an early miscarriage and a blighted ovum. During the fourth pregnancy (II.4), ultrasound scans at 20 and 21 weeks showed bilateral pleural effusions, abdominal ascites, and subcutaneous edema, having been normal at 18 weeks. At 23 weeks, a stent inserted into the left chest of the fetus extracted fluid rich in lymphocytes, consistent with a chylothorax. The baby was delivered at 38 weeks by emergency caesarean section after spontaneous labor. He required continuous positive airway pressure for a brief period, and there were small chylothoraces that resolved quickly. At 4.5 years, growth and development were normal; significant pectus excavatum with flattening of the lower part of the left hemithorax had developed since birth. AQ9

Family LE-410

The female proband (Fig. 1A) was born to distantly related Iranian parents. She was hospitalized from birth for 20 days because of meconium aspiration and respiratory problems. She had lymphedema of both legs below the knees and edema around the eyes from birth. She had pleural effusions at 3 and 5 years of age, managed by drainage and antibiotics. Spiral thorax computed tomography showed a large left pleural effusion and bilateral pleural thickening with compressive collapse of the left lower lobe. She had a fluid collection in the right knee joint at 5 years of age and was hospitalized with antibiotic treatment. At age 6 years, she had bilateral lymphedema below the ankles and papillomatosis on toes with hyperpigmentation on the dorsum of the feet and ankle area. At 20 years of age, there was bilateral lymphedema below the knees, papillomatosis on toes, hyperkeratosis of toes, and hyperpigmentation on dorsum of feet and ankle area (Fig. 1D). Echocardiography showed mild mitral valve prolapse. Twenty-four–hour Holter electrocardiogram monitoring showed 44 episodes of tachycardia.

Family LE-590

The male proband (Fig. 1A) was the first child of consanguineous Arabic parents. NIHF, with subcutaneous edema and bilateral pleural effusions, was diagnosed by ultrasound scan at 22 weeks gestation. Analysis of pleural liquid revealed a chylothorax (4×10^8/liter elements, 87% lymphocytes). Polyhydramnios was observed at 31 weeks gestation. He was born at 35 + 3 weeks, presenting with generalized

Table 1. Clinical presentation of patients carrying MDFIC variants.

Family ID	LE-452 (1)	LE-452 (2)	LE-410	LE-590	CHOP-1	LE-230	G764
Sex	Male	Male	Female	Male	Male	Male	Female
Age at presentation	19/40 weeks	20/40 weeks	Birth	22/40 weeks	20/37 weeks	Birth	35/38 weeks
Age at last exam	Died at birth (26 weeks)	6 years	20 years	Died at 7 years	4 months	10 years	11 years
Ethnicity	Chinese	Chinese	Iranian	Arabic	European	Arabic	Kurdish
Consanguineous	No	No	Yes	Yes	No	Yes	Yes (third/fourth degree)
cDNA variant	c.391dup/732 T>G	c.391dup/732 T>G	c.391dup/391dup	c.391dup/391dup	c.391dup/391dup	c.371del/371del	c.187G>T/187G>T
Amino acid change	p.(M131Nfs*3/F244L)	p.(M131Nfs*3/F244L)	p.(M131Nfs*3/M131Nfs*3)	p.(M131Nfs*3/M131Nfs*3)	p.(M131Nfs*3/M131Nfs*3)	p.(S124*/S124*)	p.(G63*/G63*)
Hydrops	Fetal, at 19 weeks	Fetal, from 20 weeks	–	Fetal, at 22 weeks	Fetal, at 20 weeks	At birth	–
Polyhydramnios	–	–		+	+		–
Chylothorax	+	+		+	+	+	+
Pleural effusions	Bilateral	Bilateral	Unilateral, recurrent	Bilateral, recurrent	Bilateral	Bilateral	Uni/bilateral, recurrent
Pericardial effusions	+	–		+	–		–
Ascites	+	+		Moderate	+		Minimal
Lymphedema	Subcutaneous	Subcutaneous	Both legs, around eyes	Both legs, subcutaneous	Subcutaneous	Generalized	Both legs, eyelids
Hydrocele	–	–		Bilateral	+	+	
Respiratory	Pulmonary hypoplasia	Respiratory support required after birth	Respiratory problems Left lower lobe collapse	Respiratory support required after birth	Required respiratory support after birth		Respiratory support required after birth
Pectus excavatum	–	Developed during infancy			–		–
Cardiac	Normal	Normal	Mitral valve prolapse, tachycardia	Cardiac arrest (age 1)	Tiny patent foramen ovale		Muscular ventricular septal defect
Ptosis	–	–			–	+	
Pleural thickening		Not known	Bilateral		–		
Hyperkeratosis	–	–	+		–		–
Inguinal hernia	–	Bilateral		+	–		–
Infections	Not applicable	–	Papillomatosis on toes	Recurrent unexplained fever Frequent upper and lower respiratory tract infections Died from septic shock (*S. pyogenes* sepsis)	Not applicable		–

subcutaneous edema, bilateral pleural effusions, and moderate ascites. He required respiratory support for 2 months and had several pleural effusions, requiring drainage. Lymphoscintigraphy did not visualize the thoracic duct. He had bilateral lower leg lymphedema, causing decreased mobility, recurrent pleural effusions, pericardial effusion, and bilateral hydroceles. At 20 months, he had cardiac and respiratory arrest requiring brief cardiorespiratory resuscitation. He had recurrent unexplained fever episodes and frequent upper and lower respiratory tract infections. He died at 7 years of age, from multiorgan failure complicating septic shock due to *Streptococcus pyogenes*.

Family CHOP-1

The 4-month-old male proband was the second pregnancy to nonconsanguineous parents of European ancestry (Fig. 1A). The prior pregnancy was stillborn due to NIHF at 23 weeks gestation. NIHF was identified in the proband on anatomy scan at 20 weeks gestational age. After birth, bilateral thoracentesis was performed confirming chylothorax. Magnetic resonance lymphangiography showed retrograde perfusion along the lower left intercostal distribution and extensive dermal backflow with bilateral groin node injection (Fig. 1E). Follow-up at 4 months of age showed asymmetric bilateral pleural effusions and asymmetric lymphedema of the bilateral lower extremities (Fig. 1E) and bilateral hydroceles.

Family LE-230

The male proband (Fig. 1A) was born to consanguineous parents of Arabic origin. At birth, he had anasarca, with generalized lymphedema and bilateral chylous pleural effusions. At 12 months of age, his generalized lymphedema had resolved, but he had stable pleural bilateral effusions. He also had ptosis and hydrocele.

Family G764

The 11-year-old female proband was the first child of third- to fourth-degree consanguineous Kurdish parents (Fig. 1A). Bilateral pleural effusions were identified at 35 weeks gestation, requiring bilateral thoracocentesis after birth by caesarean section at 38 weeks; pleural fluid analysis verified a chylothorax. The patient was discharged from hospital at 5 weeks old. At follow-up, she had recurrent asymptomatic uni- and bilateral pleural effusions, edema of the eyelids, lymphedema of the lower extremities, and minimal ascites on sonography. There were no signs of autoimmune disease.

Mdfic is prominently expressed in cardiac and lymphatic valves

To investigate the mechanisms by which *MDFIC* variants underlie hydrops fetalis and primary lymphedema, we first investigated *Mdfic* expression and localization throughout cardiovascular development in the mouse embryo. RNA in situ hybridization analyses performed in the mouse embryo at E16.5 and E18.5 revealed robust expression of *Mdfic* in the developing lung, kidney, and salivary glands (Fig. 2, A, C and D). In the cardiovascular system, *Mdfic* was detected in lymphatic and cardiac valves (Fig. 2, B and E to N). These data were confirmed by immunostaining; MDFIC protein was prominent in lymphatic and cardiac valves and appeared to be located both in the cytoplasm and in association with the extracellular matrix (ECM) of cells within these regions (Fig. 2, O to V). Given the severe lymphatic vascular phenotypes observed in patients with *MDFIC* variants, we also investigated MDFIC protein abundance in primary adult human dermal lymphatic endothelial cells (hLECs); immunoblotting revealed the presence of MDFIC and specificity of the protein species detected was confirmed by treatment of hLECs with *MDFIC* endoribonuclease-prepared, small interfering RNA (esiRNA) (fig. S1A). Subcellular fractionation of hLEC lysates confirmed that MDFIC protein was enriched in the cytoplasm and membrane compartment of these cells (fig. S1B).

$Mdfic^{M131fs*/M131fs*}$ mice exhibit profound lymphatic vascular defects and perinatal lethality

To investigate the consequences of *Mdfic* variants on cardiovascular development, CRISPR-Cas9 genome editing using a guide RNA targeting the region between c.379G and c.396C was used to generate a mouse model mimicking the most frequent human *MDFIC* truncating variant found in five of the seven patients (c.391dup/p.Met131Asnfs*3). Two founder mice were born harboring small deletions in this region, one of two base pairs and one of eight base pairs (fig. S2). Each of these variants resulted in a frameshift and premature stop codon and predicted to generate proteins 142 and 140 amino acids in length, respectively. For simplicity, these lines are referred to as $Mdfic^{M131fs*}$. Each line was backcrossed to wild-type mice for at least three generations to minimize potential off-target genome editing events, and $Mdfic^{M131fs*/+}$ mice were then crossed together to generate homozygotes. One hundred percent of homozygous $Mdfic^{M131fs*/M131fs*}$ mice exhibited perinatal lethality, with the majority dying within 30 days of birth (Fig. 3A). Careful postnatal monitoring of mice revealed that, although otherwise indistinguishable from wild-type littermates initially, immediately before death, homozygous mutant mice appeared less active, were hunched, and exhibited labored breathing. Development of symptoms was rapid and resulted in the demise of affected mice within hours of onset. Postmortem analysis of $Mdfic^{M131fs*/M131fs*}$ mice revealed chylothorax, the filling of the thoracic cavity with chylous fluid (Fig. 3B). Analysis of the lymphatic vasculature within the thoracic wall and diaphragm of $Mdfic^{M131fs*/M131fs*}$ mice with chylothorax revealed dysmorphic, distended lymphatic vessels, together with elevated numbers of LYVE1-positive macrophages (Fig. 3, D and H), phenotypes not observed in wild-type littermates (Fig. 3, C and G). Evans blue dye injection to the peritoneal cavity of $Mdfic^{M131fs*/M131fs*}$ mice revealed notable retrograde flow from the thoracic duct to the intercostal lymphatics, a phenotype reminiscent of that observed in patients with CCLA (Fig. 3, E and F). Investigation of the lymphatic vasculature in the mesentery of $Mdfic^{M131fs*/M131fs*}$ mice with chylothorax revealed no apparent leakage or breach in vessel integrity, although lymphatic vessel valves were clearly defective, appearing arrested at an early stage of development (Fig. 3, I and J). We next investigated the lymphatic vascular phenotype of postnatal $Mdfic^{M131fs*/M131fs*}$ mice before exhibiting discernibly labored breathing. In this case, chylothorax was not observed, although the lymphatic vessels in the thoracic wall were clearly enlarged and dysmorphic (fig. S3).

To investigate the nature and onset of lymphatic vessel defects in $Mdfic^{M131fs*/M131fs*}$ mice, we investigated lymphatic vessel structure and patterning during embryonic development. Analysis of lymphatic vascular patterning in the skin, diaphragm, and mesentery of E18.5 embryos revealed that the lymphatic vasculature of $Mdfic^{M131fs*/M131fs*}$ mice was wider in caliber, and greater in surface area, than the vessels of wild-type counterparts in all tissues analyzed (Fig. 4, A to I, and data file S1). In addition, valve development was

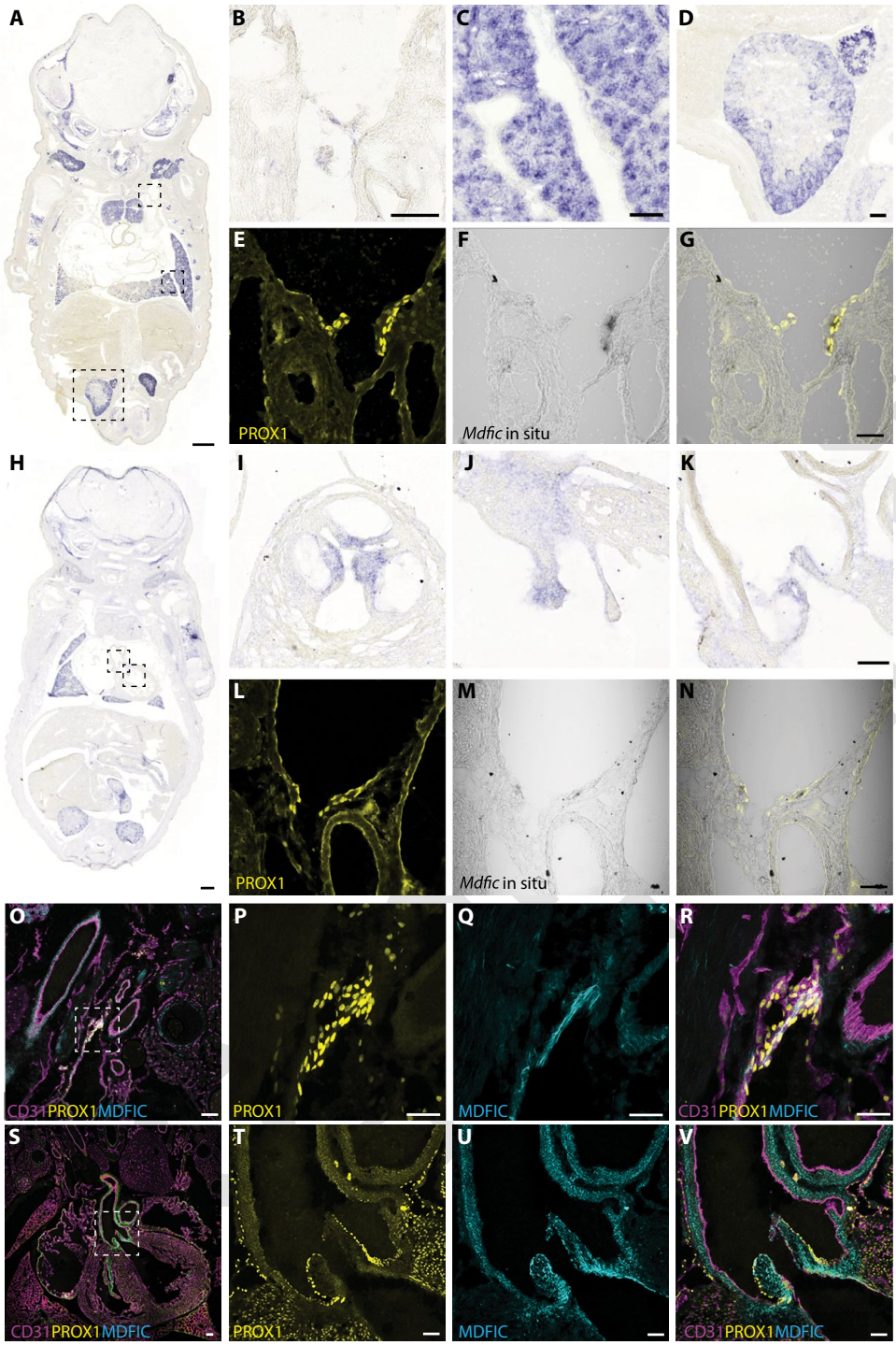

Fig. 2. *Mdfic* is prominently expressed in cardiac and lymphatic valves. RNA in situ hybridization on coronal murine E16.5 (**A** to **G**) and E18.5 (**H** to **N**) sections, demonstrating *Mdfic* expression in lymphatic valves (B, F, and G), lung (C), kidney (D), and cardiac valves (I to K). The identity of lymphatic valves in which *Mdfic* expression was detected (F, G, M, and N) was confirmed by immunostaining for PROX1 (E, G, L, and N). Immunofluorescence staining of E17.5 sections (**O** to **V**) with antibodies to PROX1 (P and T), MDFIC (Q and U), and CD31 (R and V) in lymphatic (O to R) and cardiac (S to V) valves. Scale bars, 500 μm (A and H), 200 μm (S), 100 μm (B to D, I to K, O, and T to V), 50 μm (E to G, L to N, and P to R).

abnormal in $Mdfic^{M131fs*/M131fs*}$ mice; at E18.5, significantly fewer valves were present in the mesenteric collecting lymphatic vessels of $Mdfic^{M131fs*/M131fs*}$ embryos compared with their wild-type counterparts (Fig. 4, H to J). In addition, the valves that had formed were less mature than those observed in wild-type littermates, evidenced by both the apparent arrest of valve development at the ring-like stage and by lower quantities of laminin α5 deposition in valve territories compared with wild-type counterparts (Fig. 4, K to P). Coupled with the restricted expression of *Mdfic* in valve endothelial cells, these data suggest that the primary cause of the lymphatic vascular phenotype in $Mdfic^{M131fs*/M131fs*}$ embryos is defective valve development.

The MDFIC Met131Asnfs*3 variant results in protein truncation

The most C-terminal truncating variant identified in our patient cohort (p.M131Nfs*3) results in a stop codon 95 nucleotides before the last exon/intron junction (Fig. 1, B and C), suggesting that all truncating variants may be susceptible to nonsense-mediated decay. To ascertain whether this was the case, RNA sequencing data from patients with compound heterozygous *c.391dup/c.732 T>G* (p.M131Nfs*3/p.F244L) variants were interrogated. Both variant transcripts were present at an equivalent quantity, suggesting that the *c.391dup* variant predicted to give rise to a truncated protein was not subject to nonsense-mediated decay (fig. S4A). Moreover, quantification of *MDFIC* transcripts in fibroblasts revealed comparable amounts of both *MDFIC* variant alleles in fibroblasts from the proband of LE-452 to those found in healthy controls (fig. S4B and data file S2). Analysis of *Mdfic* transcripts in the kidneys of $Mdfic^{M131fs*/M131fs*}$ mice harboring either the 2– or 8–base pair deletion also revealed that expression of the M131fs* transcript was comparable to wild-type *Mdfic* mRNA in control littermates, providing further evidence that mRNA encoding the patient *c.391dup* variant is unlikely to be degraded (Fig. 5A and data file S3). To investigate whether the predicted truncated MDFIC protein is produced and stable, we transfected human embryonic kidney (HEK) 293 cells with constructs encoding wild-type MDFIC protein or the M131fs* or Phe245Leu

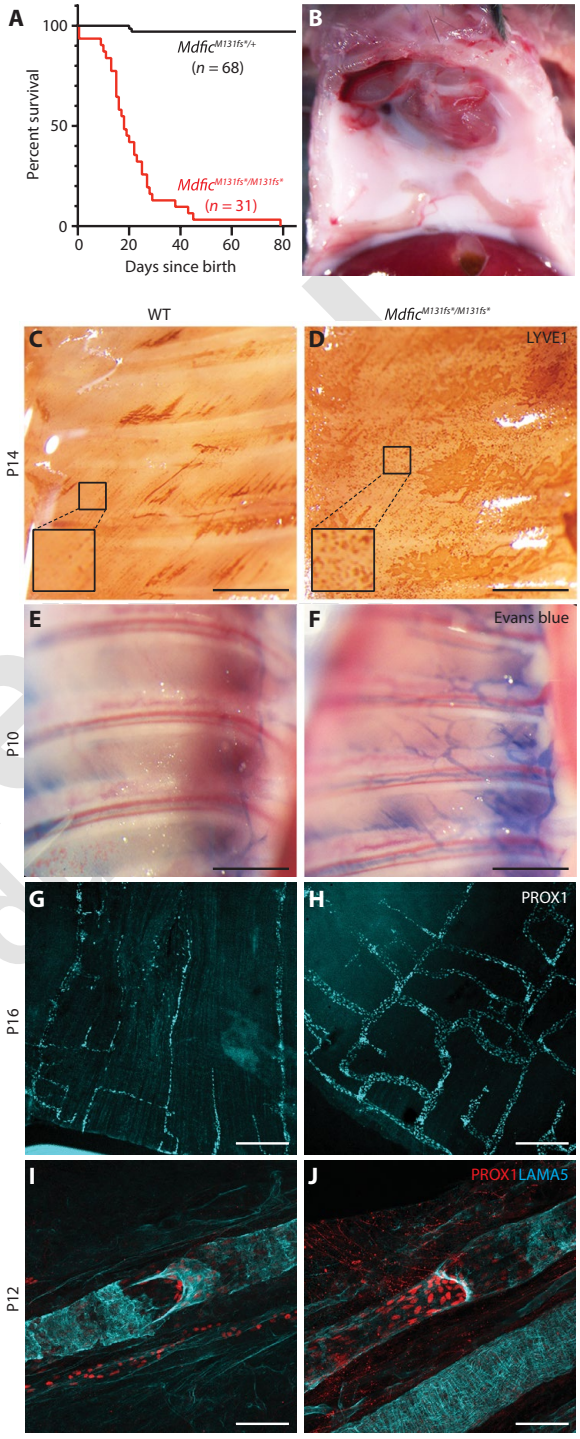

Fig. 3. *Mdfic*$^{M131fs*/M131fs*}$ mice exhibit perinatal lethality and profound lymphatic vascular defects. (**A**) Kaplan-Meier survival curve for mice with homozygous (red) and heterozygous (black) *Mdfic* truncating mutations. $n = 68$ *Mdfic*$^{+/M131fs*}$ mice, $n = 31$ *Mdfic*$^{M131fs*/M131fs*}$ mice. (**B**) Postmortem photograph of chylothorax in *Mdfic*$^{M131fs*/M131fs*}$ mice exhibiting labored breathing. (**C** and **D**) Whole-mount DAB staining of thoracic wall with an antibody to LYVE1 in *Mdfic*$^{M131fs*/M131fs*}$ mice (D) compared with WT littermates (C). Insets represent higher magnification images of the regions depicted in dashed boxes. (**E** and **F**) Photographs of Evans blue dye injection to the peritoneal cavity of P10 pups to analyze retrograde flow of dye from the thoracic duct to the intercostal lymphatics in *Mdfic*$^{M131fs*/M131fs*}$ mice (F) and WT littermates (E). (**G** and **H**) Immunofluorescence immunostaining of diaphragm with an antibody to PROX1 in *Mdfic*$^{M131fs*/M131fs*}$ mice (H) compared with WT counterparts (G). (**I** and **J**) Whole-mount immunostaining of mesenteric lymphatic vessels focusing on lymphatic valves with antibodies to PROX1 (red) and laminin α5 (LAMA5, cyan) in *Mdfic*$^{M131fs*/M131fs*}$ mice (J) compared with WT littermates (I). Scale bars, 1 mm (C to F), 200 μm (G and H), and 50 μm (I and J).

mutants (full-length mouse MDFIC protein contains one additional amino acid compared with human MDFIC; as a result, the human Phe244Leu mutant is referred to as Phe245Leu in mouse), and MDFIC protein was assessed by immunoblotting. A truncated protein corresponding to the expected size of the M131fs* (25 kDa) was detected by immunoblotting and appeared more prominent than the full-length, wild-type, and Phe245Leu proteins (32 kDa) (Fig. 5B). We also examined MDFIC protein in tissues prepared from *Mdfic*$^{M131fs*/M131fs*}$ embryos and their wild-type littermates. Using a novel antibody that we generated to mouse MDFIC, truncated MDFIC protein was detected by immunoblotting lung lysates prepared from *Mdfic*$^{M131fs*/M131fs*}$ and *Mdfic*$^{+/M131fs*}$ embryos (Fig. 5C). In contrast, full-length MDFIC was not detected in either wild-type or *Mdfic*$^{+/M131fs*}$ lungs (Fig. 5C), although the possibility exists that the full-length protein might be hidden by the nonspecific signal that was routinely detected using this antibody. These data suggest that frameshift *MDFIC* variants found in patients do not result in nonsense-mediated mRNA decay and that truncated MDFIC protein is produced and is potentially more stable than wild-type, full-length MDFIC.

MDFIC has previously been reported to tether transcription factors in the cytoplasm, thereby restricting their nuclear access and transcriptional activity (*32*–*35*). To investigate the existence of characteristic domains within MDFIC that might predict protein localization and function, the MDFIC protein sequence was subjected to analysis using several prediction programs. This analysis revealed a predicted transmembrane domain adjacent to the cysteine-rich C-terminal domain, suggesting that MDFIC might reside in membranes, consistent with our fractionation data generated in hLECs. In addition, the cysteine-rich region is highly homologous to the somatomedin B (SMB) domain of vitronectin, responsible for binding integrins, plasminogen activator inhibitor (PAI1), and the receptor for urokinase plasminogen activator (uPAR), to control cell adhesion and migration (fig. S5). We therefore sought to investigate MDFIC localization within the cell and to assess whether *MDFIC* variants found in patients affect subcellular MDFIC localization. To this end, wild-type MDFIC was ectopically expressed in HEK293 cells, which were then stained with an antibody generated to the N-terminal region of mouse MDFIC. Flow cytometric analysis revealed that MDFIC was detectable on the surface of transfected HEK293 cells, suggesting that the N-terminal region of MDFIC is located outside the cell (Fig. 6A). We next investigated the localization of the frameshift and missense MDFIC variants using the same F6

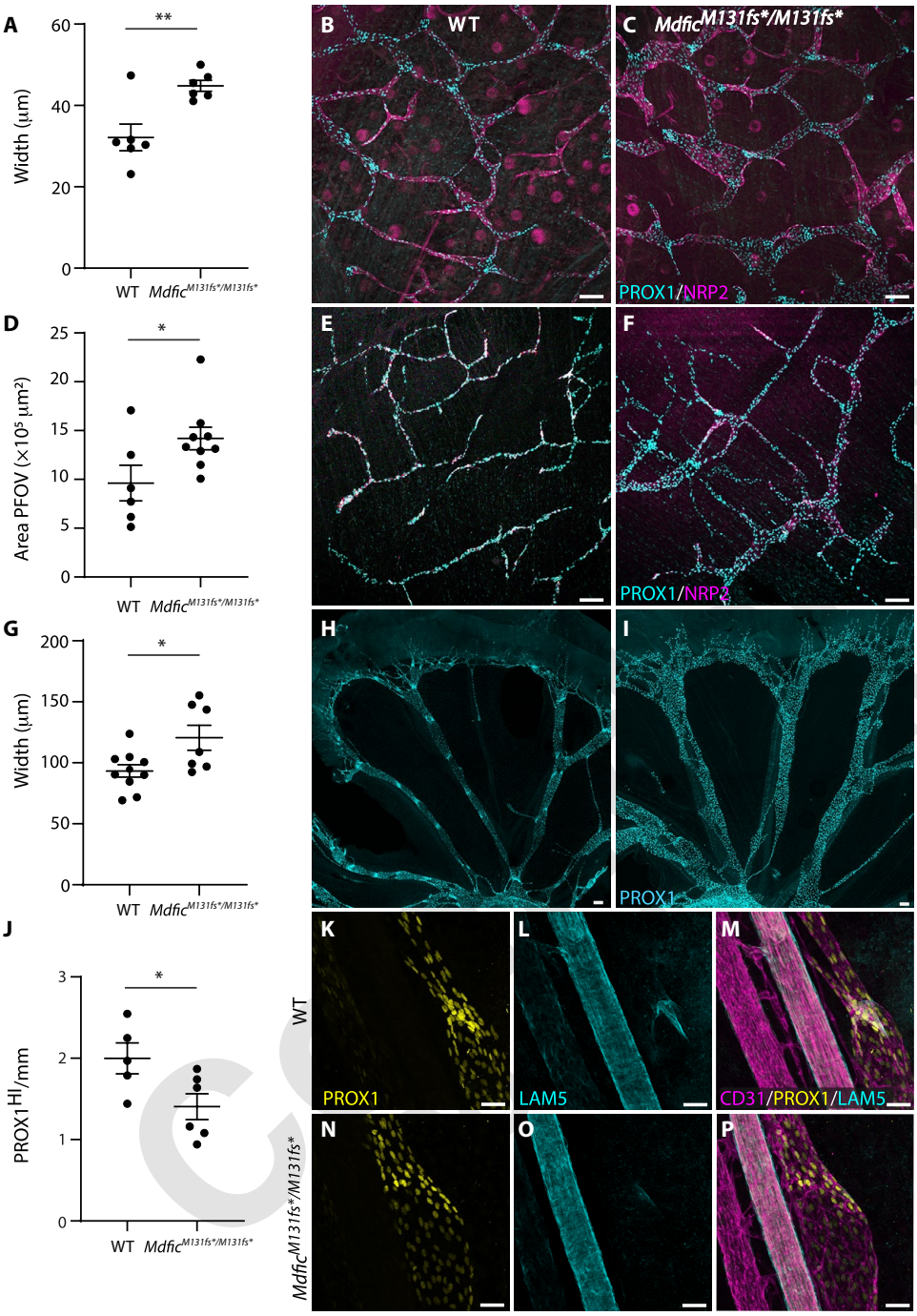

Fig. 4. E18.5 *Mdfic*$^{M131fs*/M131fs*}$ embryos exhibit distended lymphatic vessels and defective lymphatic vessel valve development. Analysis of lymphatic vessel caliber in E18.5 dermis (**A** to **C**), diaphragm (**D** to **F**), and mesentery (**G** to **I**) by whole-mount immunostaining with lymphatic markers PROX1 (cyan) and neuropilin 2 (NRP2) (magenta) in *Mdfic*$^{M131fs*/M131fs*}$ embryos (C, F, and I) compared with WT littermates (B, E, and H). Vessel width (A and G) and area (D) are quantified. Quantification of PROX1^{high} valve territories in mesenteric collecting vessels (**J**) in *Mdfic*$^{M131fs*/M131fs*}$ embryos (I) compared with WT littermates (H). Whole-mount immunostaining of mesenteric collecting vessels (**K** to **P**) with PROX1 (yellow), laminin α5 (LAMA5, cyan), and CD31 (magenta) in *Mdfic*$^{M131fs*/M131fs*}$ embryos (N to P) compared with WT littermates (K to M). Scale bars, 100 μm (B, C, E, F, H, and I), 40 μm (K to P). Error bars represent SEM, $^{*}P < 0.05$ and $^{**}P < 0.01$, calculated using two-tailed Student's *t* test. $n \geq 5$ per genotype (A, D, G, and J).

approach. The frameshift MDFIC variant that terminates before the predicted transmembrane domain (M131fs*) was not detected, suggesting that this variant protein is not present at the cell surface. In contrast, the missense variant (Phe245Leu) was detected at the cell surface in similar quantities as wild-type MDFIC (Fig. 6A). These data suggest that the MDFIC p.Met131Asnfs*3 variant is likely to act as a pathogenic loss-of-function variant with respect to membrane localization, although the possibility exists that additional functions might be gained as a result of the accumulation of truncated MDFIC protein within the cell. In contrast, we would predict that the Phe244Leu missense MDFIC variant would remain, at least in part, functional, unless this variant has a marked impact on the structure or binding capacity of the C-terminal SMB domain. To investigate the possibility that MDFIC might be secreted, medium was collected from HEK293 cells transfected with wild-type MDFIC, the MDFIC M131fs* variant, or the Phe245Leu missense variant, concentrated, and subjected to immunoblotting. Both wild-type MDFIC and MDFIC Phe245Leu were detected in the medium, whereas MDFIC M131fs* was not (Fig. 6B). Together, these data suggest that MDFIC might, at least in part, normally reside at the cell surface of valve endothelial cells and/or be secreted from valve endothelial cells to reside in the ECM and that the p.Met131Asnfs*3 variant results in truncated protein that is retained within the cytoplasm (Fig. 6C).

MDFIC stability is regulated by FOXC2, GATA2, and NFATC1

We next sought to investigate the mechanisms by which MDFIC protein is restricted to valve endothelial cells. To further explore the possibility that, as previously reported (*37*), full-length MDFIC protein is posttranslationally regulated and subject to rapid proteosomal degradation, we ectopically expressed constructs encoding full-length and M131fs* MDFIC in HeLa cells and treated cells with the proteosomal and lysosomal inhibitors MG132 and chloroquine. In contrast to untreated cells, more full-length protein was consistently detected in cells treated with these inhibitors (fig. S6); however, no notable

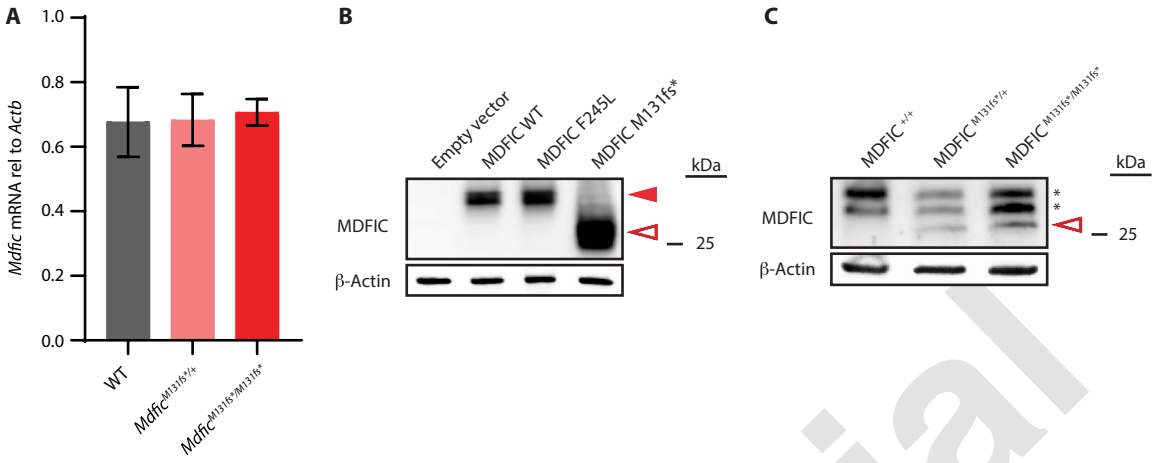

Fig. 5. The MDFIC M131fs* mutation results in protein truncation in vitro and in vivo. (**A**) Analysis of RNA isolated from kidneys of *Mdfic*$^{M131fs*/M131fs*}$, *Mdfic*$^{M131fs*/+}$, and *Mdfic*$^{+/+}$ (WT) littermates. (**B**) Immunoblotting of ectopically expressed mouse WT, M131fs*, and F245L MDFIC in HEK293 cells. Full-length (WT) MDFIC is indicated by red filled arrowhead; truncated protein is indicated by red open arrowhead. (**C**) Immunoblotting of lung protein lysates isolated from WT, *Mdfic*$^{M131fs*/+}$, and *Mdfic*$^{M131fs*/M131fs*}$ mice. Truncated MDFIC protein is indicated by red open arrowhead. Asterisks indicate nonspecific bands. Error bars represent SD, $n = 3$.

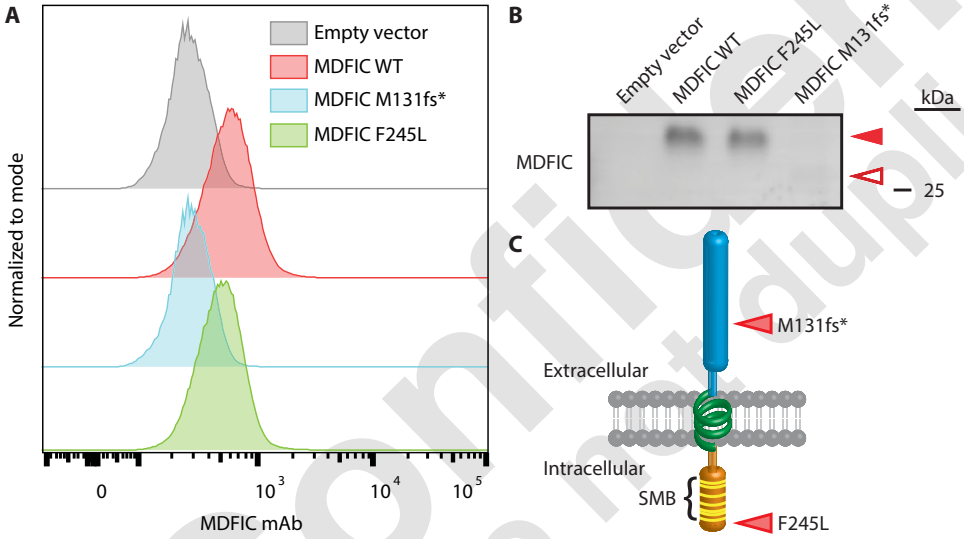

Fig. 6. MDFIC cell surface expression and secretion are abolished by the M131fs* mutation. (**A**) Flow cytometry analysis of cell surface localization of WT and mutant MDFIC variants ectopically expressed in HEK293 cells. mAb, monoclonal antibody. (**B**) Immunoblotting of concentrated conditioned medium collected from HEK293 cells ectopically expressing mouse WT MDFIC and patient variants. Red filled arrowhead indicates full-length WT MDFIC; red open arrowhead indicates truncated MDFIC. (**C**) Schematic representation of the structure and orientation of MDFIC protein in the outer membrane. MDFIC contains a predicted single-pass transmembrane domain linked to a cysteine-rich intracellular C terminus with homology to somatomedin B (SMB)–like domains. Positions of the M131fs* and F245L mutations are indicated with arrowheads.

differences in the amounts of M131fs* were observed in cells treated with MG132 and chloroquine (fig. S6). Given that MDFIC was most prominent in valves and that MDFIC has been reported to interact with multiple transcription factors, we investigated whether transcription factors present at elevated quantities in valves and important for valve development (*23*, *24*, *26*, *38*) might also influence MDFIC stability and localization. Coexpression of FOXC2, GATA2, or NFATC1 with MDFIC in HeLa cells resulted in substantially increased quantities of MDFIC detected by immunoblotting and immunostaining of transfected cells, whereas coexpression with PROX1 had no impact on the quantity of MDFIC detected (fig. S7, A, D, and E to K). Quantification of the percentage of MDFIC-positive cells in cotransfection assays revealed a statistically significant increase when MDFIC was cotransfected with FOXC2, whereas the numbers of MDFIC-positive cells when MDFIC was cotransfected with GATA2 or NFATC1 were not significantly different from control (fig. S7D and data file S4). We next investigated whether the MDFIC variant proteins found in patients were also stabilized by FOXC2, GATA2, NFATC1, or PROX1. To this end, MDFIC frameshift (M131fs*) and missense (F245L) constructs were coexpressed with FOXC2, GATA2, NFATC1, or PROX1 in HeLa cells. Consistent with the amount of variant protein detected in the lung lysates of *Mdfic*$^{M131fs*/M131fs*}$ mice, elevated quantities of M131fs* protein were detected in HeLa cell lysates compared with full-length protein (fig. S7, B and D to F), suggesting that the stability of the truncated protein is improved upon removal of the cysteine-rich C terminus or alternatively that more protein is retained within the cell. As was observed with full-length MDFIC, elevated quantities of M131fs* were detected in cells coexpressing FOXC2, GATA2, NFATC1, and, to a lesser extent, PROX1, compared with cells expressing M131fs* alone (fig. S7B), suggesting that M131fs* is likely to be stabilized or retained intracellularly in valve endothelial cells where FOXC2, GATA2, PROX1, and NFATC1 are elevated. MDFIC Phe245Leu also appeared to be stabilized by coexpression with FOXC2, GATA2, and NFATC1 (fig. S7C).

To investigate whether FOXC2, GATA2, PROX1, and NFATC1 influence MDFIC stability by binding in a complex with MDFIC,

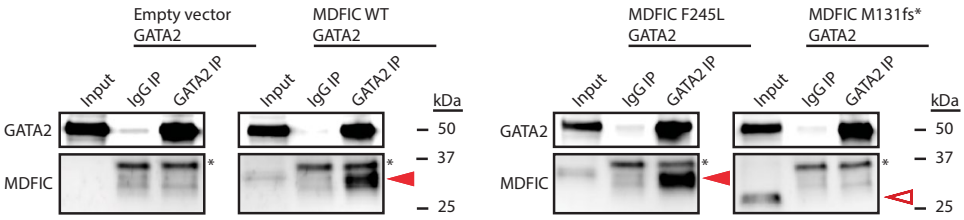

Fig. 7. Interaction between MDFIC and GATA2 proteins is interrupted by the MDFIC M131fs* mutation. WT MDFIC, M131fs*, or F245L was ectopically coexpressed with GATA2 in HEK293 cells, and immunoprecipitation was performed using an anti-GATA2 antibody. WT and F245L MDFIC proteins are indicated by red arrowheads; red open arrowhead denotes the expected size of M131fs*. Asterisks denote nonspecific band. IgG, immunoglobulin G; IP, immunoprecipitation.

MDFIC was ectopically expressed in HEK293 cells together with GATA2 or FLAG-tagged FOXC2, PROX1, or NFATC1, and transcription factors were immunoprecipitated using antibodies to GATA2 or FLAG, respectively. MDFIC coimmunoprecipitated selectively with GATA2 (Fig. 7). No coimmunoprecipitation of MDFIC with FOXC2, NFATC, or PROX1 was evident in these experiments, suggesting that FOXC2 and NFATC1 might indirectly regulate MDFIC stability (fig. S8). We next examined the impact of the MDFIC M131fs* and Phe245Leu mutants on the interaction with GATA2. Although Phe245Leu retained the ability to interact with GATA2, no interaction was detected between the M131fs* and GATA2, suggesting that the cysteine-rich C terminus of MDFIC is required to mediate the interaction with GATA2. These data suggest that a physical interaction between MDFIC and GATA2 might contribute to selective localization of MDFIC in lymphatic vessel and cardiac valves where GATA2 levels are high.

MDFIC regulates integrin β_1 activation and collective cell migration

The apparent ECM localization of MDFIC protein in valve endothelial cells in vivo, together with the cell surface localization and secretion of ectopically expressed MDFIC protein, prompted us to investigate whether MDFIC might regulate the adhesion to or migration of LECs on a variety of ECMs. To this end, primary dermal hLECs were treated with control or *MDFIC* esiRNA and plated on fibronectin, collagen I, or laminin. We first assessed the adhesion and spreading of hLECs on each of these matrices. MDFIC-deficient hLECs attached and spread more rapidly on fibronectin and collagen I and laminin than did control-treated cells (Fig. 8, A to G, and data file S5). We next investigated the consequence of MDFIC deficiency on integrin β_1 activation, a key mediator of cell attachment to the ECM. Concordant with the increased attachment of MDFIC-deficient hLECs to fibronectin, collagen I, and laminin, immunostaining of control and *MDFIC* esiRNA-treated hLECs with an antibody to activated integrin β_1 (9EG7) revealed substantially greater quantities of active integrin β_1 in MDFIC-deficient hLECs plated on these matrices (Fig. 8, H to S). We then assessed the capacity of MDFIC-deficient hLECs to undertake collective cell migration on fibronectin, collagen I, and laminin after infliction of a scratch wound. These assays revealed that MDFIC-deficient hLECs underwent significantly less migration on collagen and laminin, but not fibronectin, compared with control-treated cells (Fig. 8, T to V, and data file S5). No differences in cell proliferation were observed when MDFIC-deficient cells were plated on these ECM components (fig. S9 and data file S6). Together, these data suggest that reduction in MDFIC results in increased activation of integrin β_1, increased attachment of hLECs to their basal matrix, and, as a result, less ability to undergo collective cell migration, an important event underpinning leaflet formation during lymphatic vessel valve development.

DISCUSSION

Here, we present biallelic pathogenic variants in *MDFIC* underlying CCLA, a devastating disorder characterized by abnormalities in the development and function of major, truncal lymphatic vessels, in seven affected individuals from six independent families. By generating a novel mouse model of CCLA in which homozygous truncating variants found in human *MDFIC* were recapitulated, we have revealed a crucial role for MDFIC in the development of lymphatic vessel valves. Structural abnormalities in the lymphatic vasculature of homozygous mutant mice were observed concurrently with the onset of lymphatic vessel valve development during embryogenesis, and they progressively worsened over time, resulting in the lethality of mice due to chylothorax within the first 30 days of life. Our data reveal that biallelic *MDFIC* pathogenic variants are causative of CCLA, define a novel role for MDFIC in lymphatic vascular development, and identify a new gene important for the development and function of lymphatic vessel valves. Our work has immediate implications for improving the genetic diagnosis of patients affected by CCLA, sheds new light on the developmental etiology of CCLA, and ultimately will inform the development of novel therapeutics to combat this disease.

It is intriguing that despite the presence of valves in collecting lymphatic vessels of all tissues analyzed to date, the phenotypes of lymphatic vessel distension and, ultimately, dysfunction are predominant in the thoracic region of $Mdfic^{M131fs*/M131fs*}$ mice. All patients in our study exhibited pleural and pericardial effusions, which, in many cases, were recurrent. Chylothorax and pleural and pericardial effusions occur as a direct and severe consequence of thoracic duct dysfunction, resulting in retrograde flow of lymph into the pulmonary, cardiac, and intercostal lymphatics and fluid accumulation in the pleural/pericardial/thoracic spaces. This profound effect on the thoracic lymphatic beds may manifest as a result of the thoracic duct carrying the greatest lymph load in the body, thereby being the point at which lymphatic dysfunction reaches a threshold. In addition, the high degree of mechanical stress that the vessels of the thoracic region are subjected to during breathing, arterial pulsation, and heartbeat may result in these lymphatics being more susceptible to structural or functional impacts. Nonetheless, given that central and peripheral lymphatic symptoms are observed in patients with CCLA with *MDFIC* variants and that abnormalities in valve development are observed in the collecting lymphatics of all tissue beds analyzed in embryonic and postnatal $Mdfic^{M131fs*/M131fs*}$ mice, it is likely that lymphatic vascular defects caused by *MDFIC* pathogenic variants are prominent in all tissues.

Although our data suggest that truncating variants in *MDFIC* result in loss of MDFIC function with respect to cell surface localization and interaction with GATA2, to date, we have not identified an impact on MDFIC localization or function as a result of the missense p.Phe245Leu variant. The fact that two patients in our cohort

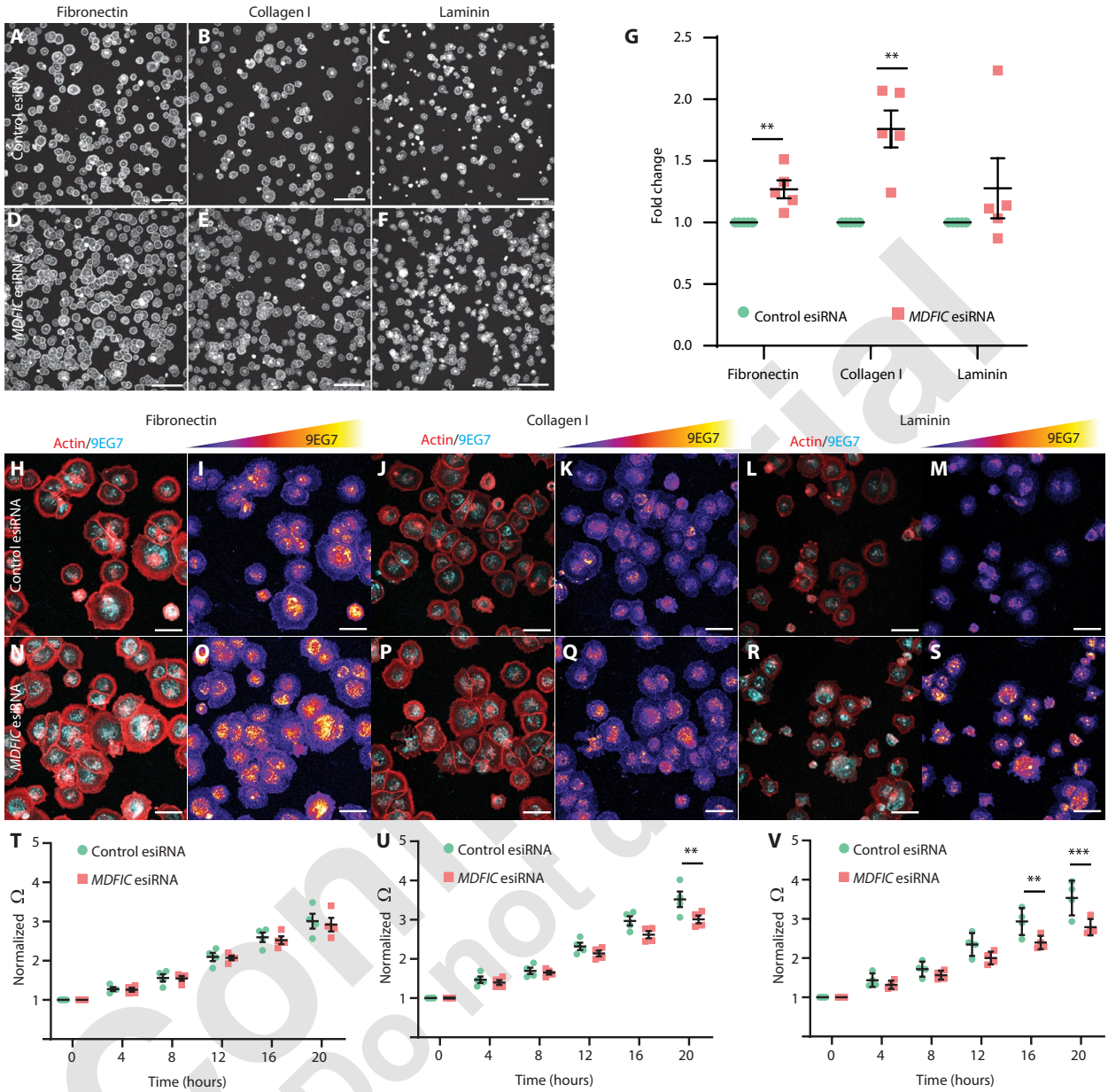

Fig. 8. MDFIC-deficient hLECs exhibit increased adhesion and decreased migration on ECM components. (**A** to **F**) Confocal microscopy of F-actin (gray) in control or MDFIC-deficient hLECs adhered to ECM components. Equal numbers of control or MDFIC-deficient cells were allowed to spread on glass wells coated with fibronectin (A and D), collagen I (B and E), or laminin (C and F) for 30 min before fixation. (**G**) Quantification of adhesion as measured by resistance. (**H** to **S**) F-actin (red) was visualized to demarcate cell area, and active integrin β_1 conformation (cyan in the left panels) was detected using the monoclonal antibody 9EG7 in control and MDFIC-deficient hLECs after attaching to fibronectin (H, I, N, and O), collagen I (J, K, P, and Q), or laminin (L, M, R, and S) for 30 min. Migration analysis of hLECs grown on ECM components, (**T**) fibronectin, (**U**) collagen I, and (**V**) laminin. Error bars represent SEM, $^{**}P < 0.01$ and $^{***}P < 0.001$, calculated using two-way ANOVA with Sidak correction. $N = 5$ independent experiments (G), $N = 4$ independent experiments (T to V). Scale bars, 200 μm (A to F) and 50 μm (H to S).

carrying compound heterozygous p.Met131Asnfs*3/p.Phe245Leu variants exhibited severe phenotypes in utero, whereas heterozygous carriers of *MDFIC* pathogenic variants are not reported to have lymphatic phenotypes, suggests that the p.Phe245Leu variant is deleterious. Although we do not yet understand the mechanism underlying dysfunction of this missense variant, the possibility exists that an important function of the C-terminal, SMB domain region is interrupted by this variant. Alternatively, when coexpressed together, there may be a dominant negative effect of the truncation mutant on the missense mutant, effectively abolishing MDFIC function, particularly as consistently elevated quantities of truncated MDFIC were observed compared with missense protein when these proteins were ectopically expressed. Future work will address these possibilities.

Similarities between the lymphatic phenotypes reported in CCLA and those described in patients with lymphatic anomalies due to pathogenic variants in components of the RAS/MAPK pathway raise the possibility that MDFIC might influence RAS/MAPK signaling

in lymphatic endothelial cells. This pathway is activated in response to major signaling axes driving lymphangiogenesis, including VEGFC/VEGFD/VEGFR3, FGF/FGFR, HGF/c-MET, and EphrinB2/EPHB4, and is reported to be important for regulating SOX18 and PROX1 quantities in lymphatic endothelial cells, thereby promoting lymphangiogenesis (*39*). Future studies will investigate whether MDFIC regulates RAS/MAPK pathway activity in the lymphatic vasculature. The observation that *Mdfic* mRNA and protein are restricted to valves in the lymphatic vasculature is also intriguing. Although the mechanisms via which *Mdfic* mRNA is selectively transcribed or stabilized in valve territories remain to be established, our data reveal that MDFIC protein coprecipitates with GATA2 and is stabilized when ectopically expressed with GATA2, FOXC2, and NFATC1. These data provide insight into the mechanisms by which MDFIC protein is detected selectively in lymphatic and cardiac valves, where these transcription factors are prominent.

How does MDFIC coordinate valve development? Mice homozygous for the truncating M131fs* pathogenic variant exhibit fewer lymphatic valves than their wild-type counterparts, and those valves that formed were arrested at an early stage of development. Our finding that MDFIC-deficient hLECs exhibit elevated quantities of activated integrin β_1, more rapid spreading on ECM components, and reduced migration suggests that the collective migration event that is important for valve development is impeded as a result of MDFIC loss of function, thereby resulting in arrested valve morphogenesis. Our observations that MDFIC is detected at the cell surface and in conditioned medium suggest that MDFIC might be an important component of the ECM in valves. Future studies will investigate the interaction of MDFIC with ECM components and determine whether this function of MDFIC is unique to lymphatic endothelial cells or conserved in other tissues in which MDFIC is prominently expressed.

In conclusion, our work uncovers homozygous and compound heterozygous pathogenic variants in *MDFIC* underlying CCLA in seven affected individuals from six independent families. We define a crucial role for MDFIC in lymphatic vessel valve morphogenesis, explaining the mechanisms by which loss-of-function pathogenic variants in *MDFIC* cause severe lymphatic vascular dysfunction and disease. Our findings will inform the genetic diagnosis of CCLA and, potentially, of additional lymphatic vascular disorders, which may manifest either in utero or postnatally. Linking MDFIC function to either the RAS/MAPK or PI3K signaling pathways has the potential to facilitate the implementation of clinically approved modulators of these pathways for patient treatment, as is being done for RAS/MAPK- and PI3K/AKT-related lymphatic and vascular anomalies (*14*, *15*, *40*, *41*) and as has been recently described for CCLA caused by an *ARAF* pathogenic variant (*6*). Future work will provide deeper insight into the mechanisms by which *MDFIC* pathogenic variants interrupt lymphatic vessel valve morphogenesis, paving the way for the development of novel, targeted therapeutics able to effectively treat severe lymphatic vascular disorders.

MATERIALS AND METHODS

Study design

The goal of this study was to investigate whether pathogenic variants in *MDFIC* are causative of lymphatic vascular anomalies and primary lymphedema. We identified *MDFIC* pathogenic variants in six families from four separate cohorts of patients with NIHF and/or primary lymphedema. No data were excluded from the study. To determine normal tissue distribution of MDFIC in mice, we used RNA in situ hybridization and immunohistochemistry (antibodies listed in table S1). To examine the consequences of the most common frameshift pathogenic variant, predicted to result in production of truncated protein, we developed a mouse model using CRISPR-Cas9 methodology and analyzed the structure and function of lymphatic vessels in animals carrying homozygous *Mdfic* pathogenic variants. We assessed the ability of MDFIC to interact with key lymphatic transcription factors by ectopic coexpression and immunoprecipitation and analyzed the effect of MDFIC pathogenic variants on protein expression, localization, and stability. We investigated the consequence of MDFIC deficiency in primary human LECs on adhesion to and migration on a variety of ECMs. Experiments using mice were approved by and conducted in accordance with guidelines of the University of Adelaide, South Australian (SA) Pathology/Central Adelaide Local Health Network (CALHN) Animal Ethics Committee, the South Australian Health and Medical Research Institute Animal Ethics committee, the University of South Australia Animal Ethics Committee, and the Australian code for the care and use of animals for scientific purposes. Patients gave informed consent in accordance with the Declaration of Helsinki under institutionally approved protocols at the Womens and Childrens Hospital (Adelaide), Universite Catholique de Louvain, Children's Hospital of Philadelphia, University Medicine Greifswald, and institutions of clinical collaborators.

Statistical analysis

Data are expressed as means ± SEM or SD, and statistical evaluation was performed using two-tailed Student's *t* test, two-way analysis of variance (ANOVA) with a Sidak multiple comparison test, or one-way ANOVA, using GraphPad Prism (version 8.2.1). *P* values less than 0.05 were considered statistically significant.

SUPPLEMENTARY MATERIALS

www.science.org/doi/10.1126/scitranslmed.abm4869
Materials and Methods
Figs. S1 to S9
Table S1
Data files S1 to S6
MDAR Reproducibility Checklist
References (*42*–*51*)

View/request a protocol for this paper from *Bio-protocol*.

REFERENCES AND NOTES

1. T. V. Petrova, G. Y. Koh, Biological functions of lymphatic vessels. *Science* **369**, (2020).
2. G. Oliver, J. Kipnis, G. J. Randolph, N. L. Harvey, The lymphatic vasculature in the 21st century: Novel functional roles in homeostasis and disease. *Cell* **182**, 270–296 (2020).
3. C. C. Trenor III, G. Chaudry, Complex lymphatic anomalies. *Semin. Pediatr. Surg.* **23**, 186–190 (2014).
4. M. Itkin, A. Chidekel, K. A. Ryan, D. Rabinowitz, Abnormal pulmonary lymphatic flow in patients with paediatric pulmonary lymphatic disorders: Diagnosis and treatment. *Paediatr. Respir. Rev.* **36**, 15–24 (2020).
5. I. Iacobas, D. M. Adams, S. Pimpalwar, T. Phung, F. Blei, P. Burrows, J. C. Lopez-Gutierrez, M. A. Levine, C. C. Trenor III, Multidisciplinary guidelines for initial evaluation of complicated lymphatic anomalies-expert opinion consensus. *Pediatr. Blood Cancer* **67**, e28036 (2020).
6. D. Li, M. E. March, A. Gutierrez-Uzquiza, C. Kao, C. Seiler, E. Pinto, L. S. Matsuoka, M. R. Battig, E. J. Bhoj, T. L. Wenger, L. Tian, N. Robinson, T. Wang, Y. Liu, B. M. Weinstein, M. Swift, H. M. Jung, C. N. Kaminski, R. Chiavacci, J. A. Perkins, M. A. Levine, P. M. A. Sleiman, P. J. Hicks, J. T. Strausbaugh, J. B. Belasco, Y. Dori, H. Hakonarson, ARAF recurrent mutation causes central conducting lymphatic anomaly treatable with a MEK inhibitor. *Nat. Med.* **25**, 1116–1122 (2019).

7. P. Brouillard, L. Boon, M. Vikkula, Genetics of lymphatic anomalies. *J. Clin. Invest.* **124**, 898–904 (2014).
8. L. Bulow, C. Lissewski, R. Bressel, A. Rauch, Z. Stark, M. Zenker, O. Bartsch, Hydrops, fetal pleural effusions and chylothorax in three patients with CBL mutations. *Am. J. Med. Genet. A* **167A**, 394–399 (2015).
9. S. Joyce, K. Gordon, G. Brice, P. Ostergaard, R. Nagaraja, J. Short, S. Moore, P. Mortimer, S. Mansour, The lymphatic phenotype in Noonan and Cardiofaciocutaneous syndrome. *Eur. J. Hum. Genet.* **24**, 690–696 (2016).
10. M. Tartaglia, E. L. Mehler, R. Goldberg, G. Zampino, H. G. Brunner, H. Kremer, I. van der Burgt, A. H. Crosby, A. Ion, S. Jeffery, K. Kalidas, M. A. Patton, R. S. Kucherlapati, B. D. Gelb, Mutations in PTPN11, encoding the protein tyrosine phosphatase SHP-2, cause Noonan syndrome. *Nat. Genet.* **29**, 465–468 (2001).
11. Y. Aoki, T. Niihori, T. Banjo, N. Okamoto, S. Mizuno, K. Kurosawa, T. Ogata, F. Takada, M. Yano, T. Ando, T. Hoshika, C. Barnett, H. Ohashi, H. Kawame, T. Hasegawa, T. Okutani, T. Nagashima, S. Hasegawa, R. Funayama, T. Nagashima, K. Nakayama, S. Inoue, Y. Watanabe, T. Ogura, Y. Matsubara, Gain-of-function mutations in RIT1 cause Noonan syndrome, a RAS/MAPK pathway syndrome. *Am. J. Hum. Genet.* **93**, 173–180 (2013).
12. P. E. Burrows, M. L. Gonzalez-Garay, J. C. Rasmussen, M. B. Aldrich, R. Guilliod, E. A. Maus, C. E. Fife, S. Kwon, P. E. Lapinski, P. D. King, E. M. Sevick-Muraca, Lymphatic abnormalities are associated with RASA1 gene mutations in mouse and man. *Proc. Natl. Acad. Sci. U.S.A.* **110**, 8621–8626 (2013).
13. A. Gallipoli, G. MacLean, J. S. Walia, A. Sehgal, Congenital chylothorax and hydrops fetalis: A novel neonatal presentation of RASA1 mutation. *Pediatrics* **147**, (2021).
14. N. Homayun-Sepehr, A. L. McCarter, R. Helaers, C. Galant, L. M. Boon, P. Brouillard, M. Vikkula, M. T. Dellinger, KRAS-driven model of Gorham-Stout disease effectively treated with trametinib. *JCI Insight* **6**, e149831 (2021).
15. T. Makinen, L. M. Boon, M. Vikkula, K. Alitalo, Lymphatic malformations: Genetics, mechanisms and therapeutic strategies. *Circ. Res.* **129**, 136–154 (2021).
16. S. Martin-Almedina, P. Mortimer, P. Ostergaard, Development and physiological functions of the lymphatic system: Insights from human genetic studies of primary lymphedema. *Physiol. Rev.* **101**, 1809–1871 (2021).
17. J. T. Wigle, G. Oliver, Prox1 function is required for the development of the murine lymphatic system. *Cell* **98**, 769–778 (1999).
18. Y. Yang, J. M. Garcia-Verdugo, M. Soriano-Navarro, R. S. Srinivasan, J. P. Scallan, M. K. Singh, J. A. Epstein, G. Oliver, Lymphatic endothelial progenitors bud from the cardinal vein and intersomitic vessels in mammalian embryos. *Blood* **120**, 2340–2348 (2012).
19. J. T. Wigle, N. Harvey, M. Detmar, I. Lagutina, G. Grosveld, M. D. Gunn, D. G. Jackson, G. Oliver, An essential role for Prox1 in the induction of the lymphatic endothelial cell phenotype. *EMBO J.* **21**, 1505–1513 (2002).
20. M. J. Karkkainen, P. Haiko, K. Sainio, J. Partanen, J. Taipale, T. V. Petrova, M. Jeltsch, D. G. Jackson, M. Talikka, H. Rauvala, C. Betsholtz, K. Alitalo, Vascular endothelial growth factor C is required for sprouting of the first lymphatic vessels from embryonic veins. *Nat. Immunol.* **5**, 74–80 (2004).
21. M. Francois, A. Oszmiana, N. L. Harvey, When form meets function: The cells and signals that shape the lymphatic vasculature during development. *Development* **148**, (2021).
22. E. Bazigou, T. Makinen, Flow control in our vessels: Vascular valves make sure there is no way back. *Cell. Mol. Life Sci.* **70**, 1055–1066 (2013).
23. T. V. Petrova, T. Karpanen, C. Norrmen, R. Mellor, T. Tamakoshi, D. Finegold, R. Ferrell, D. Kerjaschki, P. Mortimer, S. Yla-Herttuala, N. Miura, K. Alitalo, Defective valves and abnormal mural cell recruitment underlie lymphatic vascular failure in lymphedema distichiasis. *Nat. Med.* **10**, 974–981 (2004).
24. C. Norrmen, K. I. Ivanov, J. Cheng, N. Zangger, M. Delorenzi, M. Jaquet, N. Miura, P. Puolakkainen, V. Horsley, J. Hu, H. G. Augustin, S. Yla-Herttuala, K. Alitalo, T. V. Petrova, FOXC2 controls formation and maturation of lymphatic collecting vessels through cooperation with NFATc1. *J. Cell Biol.* **185**, 439–457 (2009).
25. A. Sabine, Y. Agalarov, H. Maby-El Hajjami, M. Jaquet, R. Hagerling, C. Pollmann, D. Bebber, A. Pfenniger, N. Miura, O. Dormond, J. M. Calmes, R. H. Adams, T. Makinen, F. Kiefer, B. R. Kwak, T. V. Petrova, Mechanotransduction, PROX1, and FOXC2 cooperate to control connexin37 and calcineurin during lymphatic-valve formation. *Dev. Cell* **22**, 430–445 (2012).
26. J. Kazenwadel, K. L. Betterman, C. E. Chong, P. H. Stokes, Y. K. Lee, G. A. Secker, Y. Agalarov, C. S. Demir, D. M. Lawrence, D. L. Sutton, S. P. Tabruyn, N. Miura, M. Salminen, T. V. Petrova, J. M. Matthews, C. N. Hahn, H. S. Scott, N. L. Harvey, GATA2 is required for lymphatic vessel valve development and maintenance. *J. Clin. Invest.* **125**, 2979–2994 (2015).
27. X. Geng, B. Cha, M. R. Mahamud, K. C. Lim, R. Silasi-Mansat, M. K. M. Uddin, N. Miura, L. Xia, A. M. Simon, J. D. Engel, H. Chen, F. Lupu, R. S. Srinivasan, Multiple mouse models of primary lymphedema exhibit distinct defects in lymphovenous valve development. *Dev. Biol.* **409**, 218–233 (2016).
28. A. Sabine, E. Bovay, C. S. Demir, W. Kimura, M. Jaquet, Y. Agalarov, N. Zangger, J. P. Scallan, W. Graber, E. Gulpinar, B. R. Kwak, T. Makinen, I. Martinez-Corral, S. Ortega, M. Delorenzi, F. Kiefer, M. J. Davis, V. Djonov, N. Miura, T. V. Petrova, FOXC2 and fluid shear stress stabilize postnatal lymphatic vasculature. *J. Clin. Invest.* **125**, 3861–3877 (2015).
29. R. Hagerling, Light sheet microscopy-based 3-dimensional histopathology of the lymphatic vasculature in Emberger syndrome. *Phlebologie* **49**, 242–248 (2020).
30. O. Lyons, P. Saha, C. Seet, A. Kuchta, A. Arnold, S. Grover, V. Rashbrook, A. Sabine, G. Vizcay-Barrena, A. Patel, F. Ludwinski, S. Padayachee, T. Kume, B. R. Kwak, G. Brice, S. Mansour, P. Ostergaard, P. Mortimer, S. Jeffery, N. Brown, T. Makinen, T. V. Petrova, B. Modarai, A. Smith, Human venous valve disease caused by mutations in FOXC2 and GJC2. *J. Exp. Med.* **214**, 2437–2452 (2017).
31. S. Thebault, F. Gachon, I. Lemasson, C. Devaux, J. M. Mesnard, Molecular cloning of a novel human I-mfa domain-containing protein that differently regulates human T-cell leukemia virus type I and HIV-1 expression. *J. Biol. Chem.* **275**, 4848–4857 (2000).
32. R. H. Oakley, J. M. Busillo, J. A. Cidlowski, Cross-talk between the glucocorticoid receptor and MyoD family inhibitor domain-containing protein provides a new mechanism for generating tissue-specific responses to glucocorticoids. *J. Biol. Chem.* **292**, 5825–5844 (2017).
33. D. M. Martindill, C. A. Risebro, N. Smart, M. Franco-Viseras, C. O. Rosario, C. J. Swallow, J. W. Dennis, P. R. Riley, Nucleolar release of Hand1 acts as a molecular switch to determine cell fate. *Nat. Cell Biol.* **9**, 1131–1141 (2007).
34. L. Snider, H. Thirlwell, J. R. Miller, R. T. Moon, M. Groudine, S. J. Tapscott, Inhibition of Tcf3 binding by I-mfa domain proteins. *Mol. Cell. Biol.* **21**, 1866–1873 (2001).
35. L. Snider, S. J. Tapscott, XIC is required for Siamois activity and dorsoanterior development. *Mol. Cell. Biol.* **25**, 5061–5072 (2005).
36. K. J. Karczewski, L. C. Francioli, G. Tiao, B. B. Cummings, J. Alfoldi, Q. Wang, R. L. Collins, K. M. Laricchia, A. Ganna, D. P. Birnbaum, L. D. Gauthier, H. Brand, M. Solomonson, N. A. Watts, D. Rhodes, M. Singer-Berk, E. M. England, E. G. Seaby, J. A. Kosmicki, R. K. Walters, K. Tashman, Y. Farjoun, E. Banks, T. Poterba, A. Wang, C. Seed, N. Whiffin, J. X. Chong, K. E. Samocha, E. Pierce-Hoffman, Z. Zappala, A. H. O'Donnell-Luria, E. V. Minikel, B. Weisburd, M. Lek, J. S. Ware, C. Vittal, I. M. Armean, L. Bergelson, K. Cibulskis, K. M. Connolly, M. Covarrubias, S. Donnelly, S. Ferriera, S. Gabriel, J. Gentry, N. Gupta, T. Jeandet, D. Kaplan, C. Llanwarne, R. Munshi, S. Novod, N. Petrillo, D. Roazen, V. Ruano-Rubio, A. Saltzman, M. Schleicher, J. Soto, K. Tibbetts, C. Tolonen, G. Wade, M. E. Talkowski; Genome Aggregation Database Consortium, B. M. Neale, M. J. Daly, D. G. MacArthur, The mutational constraint spectrum quantified from variation in 141,456 humans. *Nature* **581**, 434–443 (2020).
37. E. Reiss-Sklan, A. Levitzki, T. Naveh-Many, The complex regulation of HIC (human I-mfa domain containing protein) expression. *PLOS ONE* **4**, e6152 (2009).
38. R. S. Srinivasan, G. Oliver, Prox1 dosage controls the number of lymphatic endothelial cell progenitors and the formation of the lymphovenous valves. *Genes Dev.* **25**, 2187–2197 (2011).
39. Y. Deng, D. Atri, A. Eichmann, M. Simons, Endothelial ERK signaling controls lymphatic fate specification. *J. Clin. Invest.* **123**, 1202–1215 (2013).
40. A. Queisser, E. Seront, L. M. Boon, M. Vikkula, Genetic basis and therapies for vascular anomalies. *Circ. Res.* **129**, 155–173 (2021).
41. A. Van Damme, E. Seront, V. Dekeuleneer, L. M. Boon, M. Vikkula, New and emerging targeted therapies for vascular malformations. *Am. J. Clin. Dermatol.* **21**, 657–668 (2020).
42. Q. Schwarz, C. Gu, H. Fujisawa, K. Sabelko, M. Gertsenstein, A. Nagy, M. Taniguchi, A. L. Kolodkin, D. D. Ginty, D. T. Shima, C. Ruhrberg, Vascular endothelial growth factor controls neuronal migration and cooperates with Sema3A to pattern distinct compartments of the facial nerve. *Genes Dev.* **18**, 2822–2834 (2004).
43. K. L. Betterman, N. L. Harvey, Histological and morphological characterization of developing dermal lymphatic vessels. *Methods Mol. Biol.* **1846**, 19–35 (2018).
44. D. T. Sweet, J. M. Jimenez, J. Chang, P. R. Hess, P. Mericko-Ishizuka, J. Fu, L. Xia, P. F. Davies, M. L. Kahn, Lymph flow regulates collecting lymphatic vessel maturation in vivo. *J. Clin. Invest.* **125**, 2995–3007 (2015).
45. C. A. Schneider, W. S. Rasband, K. W. Eliceiri, NIH Image to ImageJ: 25 years of image analysis. *Nat. Methods* **9**, 671–675 (2012).
46. K. Hofmann, W. Stoffel, TMbase - A database of membrane spanning proteins segments. *Biol. Chem. Hoppe Seyler* **374**, 166 (1993).
47. M. Cserzo, E. Wallin, I. Simon, G. von Heijne, A. Elofsson, Prediction of transmembrane alpha-helices in prokaryotic membrane proteins: The dense alignment surface method. *Protein Eng.* **10**, 673–676 (1997).
48. H. Viklund, A. Elofsson, OCTOPUS: Improving topology prediction by two-track ANN-based preference scores and an extended topological grammar. *Bioinformatics* **24**, 1662–1668 (2008).
49. D. Juretic, L. Zoranic, D. Zucic, Basic charge clusters and predictions of membrane protein topology. *J. Chem. Inf. Comput. Sci.* **42**, 620–632 (2002).
50. C. Notredame, D. G. Higgins, J. Heringa, T-Coffee: A novel method for fast and accurate multiple sequence alignment. *J. Mol. Biol.* **302**, 205–217 (2000).
51. B. Ringelmann, C. Roder, R. Hallmann, M. Maley, M. Davies, M. Grounds, L. Sorokin, Expression of laminin alpha1, alpha2, alpha4, and alpha5 chains, fibronectin, and tenascin-C in skeletal muscle of dystrophic 129ReJ dy/dy mice. *Exp. Cell Res.* **246**, 165–182 (1999).

Acknowledgments: We thank the patients and families for their involvement in this study. We also thank C. Brown and staff at the SA Pathology Animal Facility and UniSA Core Animal Facility for animal husbandry, and L. Arriola-Martinez for assistance with analysis of RNA-seq data. We are grateful to A. Debue for technical assistance. Three of the authors of this publication are members of the Vascular Anomalies Working Group (VASCA WG) of the European Reference Network for Rare Multisystemic Vascular Diseases (VASCERN)–Project ID: 769036. We thank J. Cidlowski for the gift of the rabbit anti-human MDFIC antibody used for immunoblotting hLEC lysates, and L. Sorokin for the gift of rabbit anti-mouse laminin $\alpha 5$ antibody used for immunostaining mouse tissues. We thank T. M. Strom and the Genome Analysis Center (GAC) of the Helmholtz Zentrum München for performing whole exome sequencing for family G764. We thank K. T. Wild, E. Xu, I. Krantz, Y. Dori, and E. Pinto for patient care. This study utilized the SAHMRI Histology Slide Scanning Service (SAHMRI, Adelaide, Australia) and the Monash Antibody Technologies Facility (Monash University, Melbourne, Australia). Confocal microscopy and flow cytometry were performed at the Detmold Imaging and Flow Cytometry Facility (UniSA and SA Pathology, Adelaide, Australia). **Funding:** This work was supported by grants from the NHMRC (1146352 and 1146800 to N.L.H. and 1123341 to H.S.S.), Medical Research Future Fund (MRFF), Genomics Health Futures Mission grant ID GHFM76777 NHMRC (APP1123341), the Australian Genomic Health Alliance NHMRC Targeted Call for Research into Preparing Australia for the Genomics Revolution in Healthcare (GNT1113531) (to H.S.S. and C.B.), and the Australian Cancer Research Foundation (to H.S.S.). Additional support was provided by Cancer Council SA's Beat Cancer Project on behalf of its donors and the State Government of South Australia through the Department of Health and NHMRC Fellowship (1023059 to H.S.S.); the Australian Government Research Training Program Scholarship and the Australian Genomics Health Alliance PhD Award and NHMRC (GNT1113531 to A.B.B.); and The Hospital Research Foundation Fellowship and Royal Adelaide Hospital Mary Overton Early Career Fellowship (to P.A.). M.R. was supported by a scholarship of the Gerhard Domagk program of the University Medicine Greifswald. The South Australian Genome Editing Facility is supported by Phenomics Australia through the Australian Government's National Collaborative Research Infrastructure Strategy. These studies were also financially supported by the Fonds de la Recherche Scientifique (FNRS) grants T.0026.14, T.0247.19 (to M.V.), T.0146.16 (to L.M.B.), the Fund Generet managed by the King Baudouin Foundation (grant 2018-J1810250-211305) (to M.V.), and by la Région wallonne dans le cadre du financement de l'axe stratégique FRFS-WELBIO (WELBIO-CR-2019C-06) (to M.V.). P.B. is a Scientific Logistics Manager of the Genomics Platform of University of Louvain. We also thank the National Lottery, Belgium, and the Foundation against Cancer (2010-101), Belgium, for the support to the Genomics Platform of the University of Louvain and de Duve Institute, as well as the FNRS equipment grant U.N035.17 for the "Big data analysis cluster for NGS at UCLouvain." S.E.S. is supported by CHOP, Uplifting Athletes, and the Lymphangiomatosis and Gorham's Disease Alliance. **Author contributions:** L.M.B., D.A., E.H., L.M., and C.B. coordinated clinical phenotyping and patient treatment. M.R., U.F., and G.C.K. contributed to clinical phenotyping and analyzed data. C.L.S., K.H.W., and S.E.S. coordinated clinical phenotyping, genetic diagnosis, patient imaging, and patient treatment. E.H., D.A., A.K., N.R., L.M.B., and S.E.S. drafted the text on clinical descriptions. A.B.B., P.B., N.R., R.H., M.B., and P.A. arranged and performed genome sequencing and data analysis, drafted the text on genetics, and prepared figures and tables. D.L.S., J.K., G.A.S., S.M., A.O., K.L.B., C.N.H., P.J.B., and N.L.H. designed and performed functional experiments, analyzed the data, and prepared figures. P.Q.T., M.W., and S.G.P. designed and generated the mutant mice. N.L.H. drafted the introduction, text on functional experiments, and discussion. H.S.S., M.V., and N.L.H. conceptualized the study and analyzed the data. All authors edited and approved the manuscript. **Competing interests:** The authors declare they have no competing interests. **Data and materials availability:** All data needed to evaluate the conclusions in the paper are present in the paper and/or the Supplementary Materials. Newly created materials can be accessed by contacting the corresponding authors (M.V., H.S.S., or N.L.H.).

Submitted 21 September 2021
Accepted 4 February 2022
Published 2 March 2022
10.1126/scitranslmed.abm4869

Abstract

One-sentence summary: Pathogenic variants in *MDFIC* cause complex lymphatic anomalies because of a crucial role for MDFIC in lymphatic vessel valve development.

Editor's Summary:
Editor's summary: Variants, valve defects, and lymphatic dysfunction

Defective lymphatic vessel valve development impairs lymphatic fluid flow and contributes to lymphatic malformations, lymphedema, and related lymphatic disorders. Here, Byrne *et al.* identified mutations in *MDFIC* associated with impairments in truncal collecting lymphatic vessels in individuals with central conducting lymphatic anomaly. *Mdfic* variants disrupted lymphatic vessel patterning and valve development in mouse models, and in vitro work identified how MDFIC regulates integrin activation and collective cell migration. This work highlights the importance of lymphatic valve development and adds to our understanding of the molecular mechanisms underlying lymphatic disorders.

MS no: RAabm4869/LN/MEDICINE